

Analytic force-free jet from disk-fed rotating black holes

Luis Villarin* and Ian Vega†

National Institute of the Philippines, University of the Philippines, Diliman, Quezon City 1101, Philippines

(Dated: February 26, 2026)

We present a new analytic model of force-free electromagnetic jet launched from a disk-fed rotating black hole. The jet solution is obtained through a systematic construction from previously developed methods. The resulting physical jet solution exhibits an asymptotically parabolic structure and is parametrized by the location of localized current concentration and sign reversal in the disk. We find, however, that the jet properties show negligible dependence on the disk parameter. The black hole jet captures the basic feature of the Blandford-Znajek mechanism for energy extraction and jet formation.

I. INTRODUCTION

Astrophysical jets launched from rotating black holes are among the most energetic phenomena in our universe. They are predominantly observed in active galactic nuclei (AGN), where a supermassive black hole ($M \sim 10^5 - 10^{10} M_\odot$) steadily accretes hot gas and energetic particles and persistently emits electromagnetic radiation from radio to gamma-ray energies [1–3]. For instance, estimates of the jet power of M87* from various measurements range from 10^{42} to 10^{43} erg s⁻¹ [4, 5], about billion times more luminous than the Sun. These jets are widely believed to be driven by large-scale, strong magnetic fields that observationally thread the horizon [6]. The accretion disk surrounding the black hole serves as the source of these magnetic fields, as the infalling gas is thought to become highly magnetized due to friction and relativistic velocities [7]. Numerical simulations have strengthened this view that relativistic jets arise from poloidal magnetic fields generated by accretion flows onto black holes [8, 9]. However, the question how these strong magnetic fields extract energy from the black hole remains.

The Blandford–Znajek (hereafter, BZ) mechanism [10] is the prevailing theory for energy extraction from rotating black holes. BZ showed that when the plasma’s stress-energy density is negligible compared to that of the electromagnetic field in a stationary axisymmetric black hole magnetosphere, the black hole’s rotational energy can be extracted by magnetic fields threading the horizon, in a manner analogous to a Penrose process [11]. In this regime, where plasma inertia and pressure are negligible relative to the electromagnetic energy and stresses, the magnetosphere is well described by force-free electrodynamics (FFE). Within this framework, the energy extraction process is determined entirely by the structure of the magnetic field and independent of the plasma microphysics and detailed magnetohydrodynamic processes. Also, although FFE was first introduced in astrophysical context through pulsar magnetosphere model, its application to rotating black holes is distinguished by the

requirement that the electromagnetic fields satisfy a regularity condition at the horizon [12].

While numerical simulations are more accessible and insightful, analytic solutions to black hole force-free electrodynamics remain indispensable for enforcing horizon regularity conditions, informing numerical implementations, and ensuring global consistency. However, the equations governing FFE in Kerr spacetime appear analytically intractable, even when stationarity and axisymmetry are assumed, and exact, physically realistic solutions remain scarce. Some FFE solutions in the Kerr background are known [13, 14], with only a handful describing force-free jets from disk-accreting rotating black holes [10, 15]. These disk-fed black hole jet solutions are obtained at first order in the black hole spin parameter, using the Blandford–Znajek perturbation method [10], in which the properties of the poloidal magnetic field are expressed as power series in the spin parameter. In the first-order of this perturbation, the magnetic flux function corresponds to a known vacuum solution in Schwarzschild spacetime, while the angular velocity and the poloidal current are linear in the angular velocity of the horizon, and are to be determined by regularity and boundary conditions. In the model of the black hole hyperbolic jet, a vacuum solution in flat spacetime was first derived and promoted to Schwarzschild spacetime via a unique, canonical mode-mode mapping before applying the BZ perturbation method [16]. However, the perturbation method requires careful treatment, as inconsistencies in the expansion have been identified, for example in the monopole solution [17], and ambiguities in the boundary condition at infinity are need to be resolved on a case-by-case basis [18].

In addition, recent developments have highlighted the importance of the underlying geometric structure of spacetime in force-free electromagnetic fields that open new avenues for the construction of analytic FFE solutions. Building on the covariant formulation of FFE introduced by Uchida [19], Gralla and Jacobson [20] developed a fully spacetime-covariant approach to FFE. In this formulation, FFE fields are emphasized to be so-called degenerate field, allowing them to be understood in terms of two-dimensional foliations of spacetime. In the magnetically-dominated case, these foliations represent the time evolution of magnetic field lines, along which

* jlvillarin@nip.upd.edu.ph

† ivega@nip.upd.edu.ph

particles are confined to.

Moreover, Menon [21] further established the connection between foliations in the background spacetime and the force-free field. In this new formalism, the foliations can be described in terms of the tetrad of an inertial frame on the background spacetime. He then showed a condition on the geometry of the foliations in terms of the tetrad that a force-free field has to satisfy. Adhikari et al. [13] exploited this geometric approach to build new exact solutions in Kerr background by noting that inertial frames are generally connected with each other via a Lorentz transformation. But, in general, exploiting this approach comes also with analytic difficulties comparable to those encountered in solving the highly nonlinear force-free equations in Kerr spacetime. We suspect though that it is especially effective in flat spacetime, as demonstrated in this paper.

In this paper, we build a novel analytic force-free jet model around a disk-fed rotating black hole. The model arises from a systematic construction of force-free solutions rather than from first principles. We combine previous methods to arrive at our jet model: deriving a new vacuum solution in flat spacetime using similar approach in [13] from the hyperbolic solution, promoting the solution to Schwarzschild background by the unique canonical mapping introduced in [16], and performing the BZ perturbative method. Explicitly, we begin by deriving previously unexplored vacuum degenerate fields in flat spacetime sourced by thin magnetized disk. Among these solutions, we identify a physically-reasonable solution, parameterized by the location of sign reversal and concentration of current in the disk, that exhibits asymptotically parabolic magnetic fields while avoiding pathological current divergences that render the other solution we found unphysical. We then promote this solution to the Schwarzschild background by first expanding it near the origin and at infinity, and subsequently applying the canonical mapping. Then, we seeded it to the BZ perturbation method in the first order in the black hole spin. Afterwards, we finally impose the horizon regularity condition and a well-established asymptotic behavior on the solution to determine the angular velocity and poloidal current of the jet.

This paper is organized as follows. In Sec. II, we review force-free electrodynamics from a geometric perspective, focusing on degenerate Maxwell fields and spacetime foliations. We also discuss exact vacuum solutions in flat spacetime that would be useful in the construction of our jet solution. In Sec. III, we derive new vacuum degenerate solutions from the hyperbolic solution using the geometric methods mentioned earlier. In Sec. IV, we promote the expansions of the solution to Schwarzschild spacetime and perform the BZ perturbation method. Then, we complete the angular velocity and poloidal current associated with the jet. Finally, we analyze the properties of the black hole jet, including its angular velocity profile, current distribution, total electromagnetic energy flux, and effective resistance. Our metric signature is al-

ways $(-, +, +, +)$ and we work in Heaviside-Lorentz and geometrized units ($G = c = \mu_0 = 1$). Also, our orientation in flat spacetime with cylindrical coordinates (t, z, ρ, φ) is $dt \wedge dz \wedge d\rho \wedge d\varphi$.

II. THEORY OF FORCE-FREE FIELD

In the first two parts of this section, we briefly review the covariant spacetime formulation and the spacetime geometric structure of force-free electrodynamics, following Refs. [20] and [21]. We conclude this section by discussing the mapping of vacuum fields from flat to Schwarzschild spacetime, which is relevant for the analytic derivation of our analytic jet model.

A. Force-free electrodynamics

In a force-free setting, the electromagnetic four-force density is zero,

$$F_{ab}j^b = 0, \quad (1)$$

where F_{ab} is the Faraday 2-form and j^a is the four-current. Together with the Maxwell's equations,

$$\nabla_{[a}F_{bc]} = 0, \quad (2)$$

$$\nabla_b F^{ab} = j^a, \quad (3)$$

the force-free electrodynamics can be expressed as

$$\nabla_{[a}F_{bc]} = 0, \quad F_{ab}\nabla_c F^{bc} = 0. \quad (4)$$

In the language of differential forms, the Maxwell's equations are written as

$$dF = 0, \quad (5)$$

$$d * F = J, \quad (6)$$

where ‘*’ denotes the Hodge dual with respect to the background spacetime¹.

The homogeneous Maxwell equations (5) state that the Faraday 2-form is closed. Although not all closed forms are globally exact, we may ‘locally’ write $F = dA$ for some potential one-form A . In force-free electrodynamics, however, the field admits a particular structure.

Force-free fields are under the degenerate fields that obey the condition

$$F_{[ab}F_{cd]} = 0, \quad (7)$$

¹ The Faraday tensor is written as $F = \frac{1}{2} F_{ab} dx^a \wedge dx^b$, and the current-charge three-form J are related to the four-current via $j^a = \frac{1}{6} \epsilon^{abcd} J_{bcd}$.

This condition states that a degenerate field is written as a wedge product of two one-forms,

$$F = \alpha \wedge \beta. \quad (8)$$

The degeneracy of force-free field can be realized by rewriting the force-free condition as

$$F_{[ab}F_{cd]}J^d = 0. \quad (9)$$

Also, this condition amounts to the vanishing of the Lorentz scalar $\vec{E} \cdot \vec{B}$ in a local frame.

From the degeneracy condition and the homogeneous Maxwell equations, a force-free field is generally given by

$$F = d\phi_1 \wedge d\phi_2, \quad (10)$$

where ϕ_1, ϕ_2 are functions called the *Euler potentials*. We may rephrase the force-free condition as

$$F_{a[b}J_{cd]} = 0, \quad (11)$$

and with Eq. (10), the Euler potentials should then satisfy the equations,

$$d\phi_1 \wedge J = 0 = d\phi_2 \wedge J. \quad (12)$$

The remaining equations to be satisfied are the inhomogeneous equations that finally provide the complete description of the force-free electrodynamics,

$$d\phi_i \wedge d * (d\phi_1 \wedge d\phi_2) = 0, \quad i = 1, 2. \quad (13)$$

Obviously, a vacuum degenerate Maxwell field automatically satisfies Eq. (13), hence it is trivially force-free. In what follows, we refer to a vacuum degenerate Maxwell field simply as a vacuum degenerate field.

B. Geometric structure

The Euler potentials determine the nature of the force-free field. By taking $(d\phi_1)_a$ and $(d\phi_2)_a$ to be orthogonal, the magnitude of the field strength is

$$F^2 = F_{ab}F^{ab} = 2(B^2 - E^2) = 2\|d\phi_1\|^2\|d\phi_2\|^2, \quad (14)$$

where $\|\alpha\|^2 = g^{ab}\alpha_a\alpha_b$ is the squared-norm. Since there are no two orthogonal timelike vectors, the field is magnetically dominated ($F^2 > 0$) if and only if both vectors $(d\phi_1)^a$ and $(d\phi_2)^a$ are spacelike. This describes a force-free magnetosphere and there is always a Lorentz frame where the electric field vanishes. Accordingly, we restrict attention to magnetically-dominated from this point forward.

The degeneracy of force-free field has profound geometric spacetime structure. At each point, there exists a two-dimensional vector space that annihilates the force-free field, namely the kernel of F , denoted as $\ker F$. The $\ker F$ is orthogonal to the space spanned by vectors $(d\phi_1)^a$ and $(d\phi_2)^a$, and forms an involutive distribution. By Frobenius theorem, it can easily be shown that

the distributions are tangent to two-dimensional integral submanifolds. The submanifolds foliate the spacetime, and are called *field sheets* by Gralla and Jacobson [20], and *flux surfaces* by Uchida [19]. In force-free magnetospheres, these submanifolds are Lorentzian and describe the spacetime evolution of the magnetic field lines.

Menon [21] established a geometric correspondence between force-free field sheets and local inertial frames on a spacetime manifold M . At each point $p \in M$, there exists a local inertial frame (e_0, e_1, e_2, e_3) defined on an open set U_p of p such that the timelike basis e_0 and spacelike basis e_1 span the $\ker F$ associated with the field sheet restricted to U_p . Then, the mean curvature field on the field sheet is expressed as

$$H = \frac{1}{2}\{-\Pi(e_0, e_0) + \Pi(e_1, e_1)\}, \quad (15)$$

where Π is the *extrinsic curvature* or the *second fundamental form* of the sheet that takes tangent vector fields, say V and W , and give

$$\Pi(V, W) = (\nabla_V W)^\perp. \quad (16)$$

The symbol \perp denotes the projection operator that takes the normal component of the vector on the field sheet. We can also define a ‘dual’ mean curvature on the orthogonal distribution to the field sheet, spanned by e_2 and e_3 , even if the distribution is not involutive, as

$$\tilde{H} = \frac{1}{2}\{\Pi(e_2, e_2) + \Pi(e_3, e_3)\}. \quad (17)$$

Menon proved that, up to a constant in h , the electromagnetic field in Eq. (10), rewritten as

$$F = h e_2^b \wedge e_3^b, \quad (18)$$

with the dual field

$$*F = h e_0^b \wedge e_1^b, \quad (19)$$

is the unique magnetically-dominated force-free field, if and only if,

$$dH^b + d\tilde{H}^b = 0, \quad (20)$$

where ‘ b ’ denotes musical isomorphism. As a corollary,

$$d(\ln h) = 2(H^b + \tilde{H}^b). \quad (21)$$

Eqs. (20) and (21) are statements that $H^b + \tilde{H}^b$ should be closed and exact. Following this theorem may also provide degenerate vacuum fields.

C. Degenerate vacuum fields

Although vacuum degenerate fields are trivial solutions of the force-free equations, they provide a natural starting point for perturbative constructions of solutions in

Kerr spacetime, such as in the Blandford-Znajek perturbation method. Gralla, Lupsasca, and Rodriguez [16] derived a first-order $\mathcal{O}(a)$ jet solution in the spin parameter a of a black hole by extending a known vacuum solution in flat to Schwarzschild spacetime and performing the BZ perturbation method. In the following sections, we adopt a similar procedure after first identifying an interesting vacuum field in flat spacetime using the preceding theorem. Here, we briefly discuss the canonical mapping of vacuum degenerate solutions in flat spacetime to corresponding solutions in the Schwarzschild spacetime. We work with stationary, axisymmetric fields, which are relevant for the discussions of energy extraction from a rotating black hole. This section is mainly a revisit of Appendix B of Ref. [16].

A stationary axisymmetric force-free field in a background spacetime that shares the same symmetry is fully characterized by three scalar functions: the magnetic flux function $\psi(r, \theta)$, angular velocity of the poloidal field lines $\Omega_F(\psi)$, and total poloidal electric current $I(r, \theta)^2$. The flux function and the poloidal magnetic field lines uniquely determine one another, and the latter define two-surface foliations of spacetime. It means that the magnetic flux function depends only on the level set function of a poloidal curve, represented by $u(r, \theta)$ for instance. Under level-set reparametrization, $u \rightarrow f(u)$, the force-free equation is covariant and the flux function is invariant. Only a handful of classical curves are known to represent force-free magnetospheres around black holes.

In terms of the three functions, the force-free field in flat spacetime is written as³

$$2\pi F = d\psi \wedge [d\varphi - \Omega_F dt] + \frac{I}{\rho} dz \wedge d\rho. \quad (22)$$

The toroidal component of the force-free equation (13) implies $I = I(\psi)$, meaning that the current flows along the magnetic field lines. Meanwhile, the poloidal component of the force-free equation is a second-order, non-linear partial differential equation relating ψ , $\Omega_F(\psi)$ and $I(\psi)$, and is called the *stream equation* or *Grad-Shafranov equation*.

In the vacuum case ($I = \Omega_F = 0$), a stationary axisymmetric field is then given by

$$2\pi F = d\psi(r, \theta) \wedge d\varphi. \quad (23)$$

The linear superposition of such fields remain degenerate and stationary axisymmetric.

The stream equation in the vacuum case in flat spacetime reduces to

$$r^2 \partial_r^2 \psi + \partial_\theta^2 \psi - \cot \theta \partial_\theta \psi = 0, \quad (24)$$

whereas in the Schwarzschild spacetime it becomes

$$r(r - 2M) \partial_r^2 \psi + 2M \partial_r \psi + \partial_\theta^2 \psi - \cot \theta \partial_\theta \psi = 0, \quad (25)$$

where M is the Schwarzschild mass. We can make an identification between the solutions of Eqs. (24) and (25) as the two equations admit separation into radial and angular components, share the same angular equations, and agree entirely in the limits $r \rightarrow \infty$ or $M \rightarrow 0$, upon identifying the flat spacetime coordinates with the Schwarzschild coordinates. By writing the flux function as $\psi_l \propto R_l(r) \Theta_l(\theta)$, Eq. (25) separates into

$$\frac{d}{d\theta} \left(\frac{1}{\sin \theta} \frac{d\Theta_l}{d\theta} \right) + \frac{l(l+1)}{\sin \theta} \Theta_l = 0, \quad (26)$$

$$\frac{d}{dr} \left[\left(1 - \frac{2M}{r} \right) \frac{dR_l}{dr} \right] - \frac{l(l+1)}{r^2} R_l = 0, \quad (27)$$

where $l(l+1) > 0$ serves as a separation constant. The radial equation in flat spacetime is obviously the $M = 0$ case of Eq. (27), while the angular equation remains the same.

The angular equation (26) is of Sturm-Liouville form, and its eigenfunctions can be classified into odd modes with $l = 2k - 1$ and even modes with $l = 2k$, where k is a positive integer. Imposing the condition that the eigenfunctions vanish at the poles, they form a complete set that is mutually orthogonal with respect to the weight $csc \theta d\theta$. The solutions are given by the following:

$$\Theta_{2k-1}(\theta) = {}_2F_1[k - 1/2, -k, 1/2, \cos^2 \theta], \quad (28)$$

$$\Theta_{2k}(\theta) = {}_2F_1[k + 1/2, -k, 3/2, \cos^2 \theta] \cos \theta. \quad (29)$$

The $l = 0$ angular solution is excluded from the set of the eigenfunctions since it is not orthogonal to all of them.

Meanwhile, the radial equation in flat spacetime has two kind of solutions: solutions that are regular at the origin (but not at infinity), r^{l+1} , and regular at infinity (but not at the origin), r^{-l} . Analogous radial solutions exist in Schwarzschild spacetime that are regular only at the horizon, $R_l^<$, or at infinity, $R_l^>$. These can be normalized such that, in the limit $r \rightarrow \infty$ or $M \rightarrow 0$, they reduce to the corresponding flat spacetime solutions, i.e., $R_l^< \rightarrow r^{l+1}$ and $R_l^> \rightarrow r^{-l}$. These radial solutions are presented in Ref. [16], and here we provide an algebraic simplification for $R_l^>(r)$, as follows

$$R_l^<(r) = \frac{r^2}{2} (-2M)^{l-1} \frac{\Gamma(l+2)^2}{\Gamma(2l+1)} \times {}_2F_1 \left[l+2, 1-l; 3; \frac{r}{2M} \right], \quad (30)$$

² We refer the reader to Sec. 7 of Ref. [20] for a detailed discussion of the poloidal and toroidal decomposition of stationary, axisymmetric spacetimes, as well as the general stationary, axisymmetric fields.

³ The corresponding Euler potentials are $\phi_1 = \psi(r, \theta)$ and $\phi_2 = \psi_2(r, \theta) + \varphi - \Omega_F(\psi)t$. The function I appears on the Faraday two-form by redefinition from ψ_2 . Also, we use the convention from Ref. [16].

$$R_l^>(r) = \frac{2}{\sqrt{\pi}} \left(\frac{r}{4}\right)^{-l} \frac{\Gamma(l + \frac{3}{2})}{(l+1)\Gamma(l)} \times \sum_{i=0}^{\infty} \frac{\Gamma(l+i)\Gamma(l+i+2)}{\Gamma(2l+2+i)\Gamma(i+1)} \left(\frac{2M}{r}\right)^i \quad (31)$$

$$= r^{-l} {}_2F_1 \left[l, l+2, 2l+2, \frac{2M}{r} \right], \quad (32)$$

with $r > 2M$. We obtained simplification to $R_l^>(r)$ by expanding the expression inside the braces of Eq. B.12 in Ref. [16] about $2M/r = 0$, and resumming the result to obtain Eq. (32).

III. VACUUM FIELDS

Any other local inertial frame can be generated from a known tetrad (e_0, e_1, e_2, e_3) on a background spacetime via a spacetime-dependent homogeneous Lorentz transformation $\Lambda(x)$,

$$\begin{pmatrix} \bar{e}_0 \\ \bar{e}_1 \\ \bar{e}_2 \\ \bar{e}_3 \end{pmatrix} = \Lambda(x) \begin{pmatrix} e_0 \\ e_1 \\ e_2 \\ e_3 \end{pmatrix}, \quad (33)$$

where Λ satisfies $\eta = \Lambda^T \eta \Lambda$. Given a known inertial frame or a frame associated to a force-free solution, one may use the theorem of Sec. II to construct a new force-free field via an appropriate Lorentz transformation. In general, this procedure does not guarantee the existence of a new physically meaningful solution, since one must still provide a transformed tetrad that follows the condition in (21) and (22), without regard to any regularity conditions. Nevertheless, it provides a systematic method for constructing new exact solutions in arbitrary background spacetimes. For example, Adhikari, Menon, and Medvedev [13] applied this method in Kerr spacetime and succeeded in constructing new exact solutions.

In flat spacetime, the only transformation that can generate a new vacuum solution from the tetrad of a known one is an orthogonal transformation in the poloidal plane. To the best of our knowledge, an explicit proof of this simple statement has not been presented in the literature, and we therefore provide one in Appendix A. But, in this work, we only consider the improper rotation

$$\Lambda(x) = \begin{pmatrix} 1 & 0 & 0 & 0 \\ 0 & \frac{1}{\sqrt{1+L^2}} & \frac{L}{\sqrt{1+L^2}} & 0 \\ 0 & \frac{L}{\sqrt{1+L^2}} & -\frac{1}{\sqrt{1+L^2}} & 0 \\ 0 & 0 & 0 & 1 \end{pmatrix}, \quad (34)$$

where L is a function of the poloidal coordinates.

In this section, we perform the same method to the vacuum hyperbolic solution in flat spacetime that models a field in the presence of a disk around a compact object. The hyperbolic solution is parametrized by an inner disk radius, but this parameter acquires a different physical interpretation in the new solutions constructed here.

A. Parametrized solutions

Among known vacuum fields in flat spacetime, the hyperbolic field is unique in being parametrized by the inner radius of a magnetized disk surrounding a compact object; for this reason, we choose it as our seed solution. The solution can alternatively be obtained using the foliation-dependent method, in which an output from a function-builder describing a possible force-free poloidal curve is checked to determine whether it satisfies the universal ‘foliation condition’ derived in Ref. [22].

The hyperbolic level set function on which the magnetic flux depends, in cylindrical coordinates, is

$$u = \frac{\sqrt{(\rho+d)^2 + z^2} - \sqrt{(\rho-d)^2 + z^2}}{2d}, \quad (35)$$

where d is the inner disk radius. The magnetic flux function of the hyperbolic solution in the vacuum case is

$$\psi(u) = \psi_0(1 - \sqrt{1-u^2}), \quad (36)$$

where ψ_0 is a constant factor⁴. The radial and vertical fields arise as special cases of the hyperbolic solution in the limits $d \rightarrow 0$ and $d \rightarrow \infty$, respectively. The tetrad corresponding to the foliation of the spacetime due to the vacuum field is given by

$$\begin{pmatrix} e_0 \\ e_1 \\ e_2 \\ e_3 \end{pmatrix} = \begin{pmatrix} \partial_t \\ \rho \sqrt{\frac{1-u^2}{\rho^2 - d^2 u^4}} \partial_z + u \sqrt{\frac{\rho^2 - d^2 u^2}{\rho^2 - d^2 u^4}} \partial_\rho \\ u \sqrt{\frac{\rho^2 - d^2 u^2}{\rho^2 - d^2 u^4}} \partial_z - \rho \sqrt{\frac{1-u^2}{\rho^2 - d^2 u^4}} \partial_\rho \\ \partial_\varphi \end{pmatrix}. \quad (37)$$

Applying the rotation defined in Eq. (34) to the given tetrad, we find a partial differential equation of the function L , equivalent to the condition (20). Remarkably, we were able to solve the equation exactly, and found that the solutions are giving exact $H^b + \tilde{H}^b$. These solutions are

$$L_1 = \frac{u\rho}{(1 + \sqrt{1-u^2})\sqrt{\rho^2 - d^2 u^2}}, \quad (38)$$

$$L_2 = -\frac{u}{2\rho} \frac{\rho^2 - d^2 u^2(2-u^2)}{\sqrt{(1-u^2)(\rho^2 - d^2 u^2)}}. \quad (39)$$

⁴ The hyperbolic solution has an exact rotating counterpart in flat spacetime.

For each field defined by the tetrads resulting from these transformations, we write the magnetic flux function as $\psi(v) = \psi_0 v$. Then, the corresponding level set functions for the two solutions are

$$v_1 = \frac{u\sqrt{\rho^2 - d^2 u^2}}{1 + \sqrt{1 - u^2}}, \quad (40)$$

$$v_2 = \frac{u^3\sqrt{\rho^2 - d^2 u^2}}{\rho^2 - d^2 u^4}, \quad (41)$$

One can easily verify that these solutions indeed satisfy the vacuum stream equation in flat spacetime. These solutions were not found in Ref. [22], however, using the foliation-dependent method, as the function-builder used were unable to include the functions (40) and (41) in the process.

The two flux functions are well-defined throughout the flat spacetime and vanishes at the axis of symmetry, thereby preventing any line current there. This is obvious for Eq. (40); for Eq. (41), we can rewrite and simplify the function in cylindrical coordinates to find the expression that is also well-defined at the z -axis. However, unlike some known vacuum solutions in flat spacetime, we do not find any rotating counterparts of these two solutions that describe pulsar force-free fields. Nonetheless, the focus of this paper is on force-free field in the vicinity of a black hole.

As $d \rightarrow \infty$, the foliation of external quadrupole, or the X-point⁵, solution arises in the two solutions,

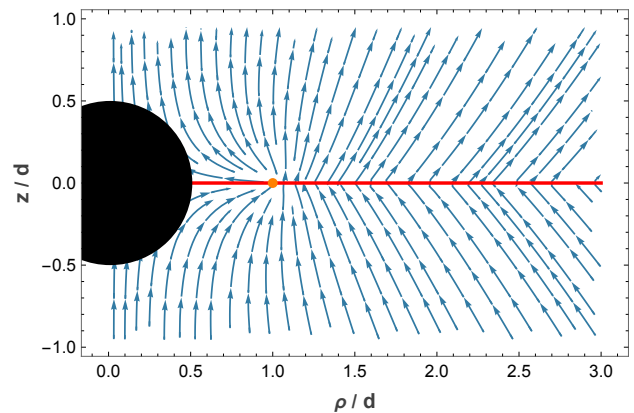
$$\lim_{d \rightarrow \infty} 2d^2 v_1 = \lim_{d \rightarrow \infty} d^4 v_2 = \rho^2 z = r^3 \sin^2 \theta \cos \theta. \quad (42)$$

However, the two solutions result in different foliations as $d \rightarrow 0$. In this limit, v_1 becomes parabolic, while v_2 becomes dipolar as follows:

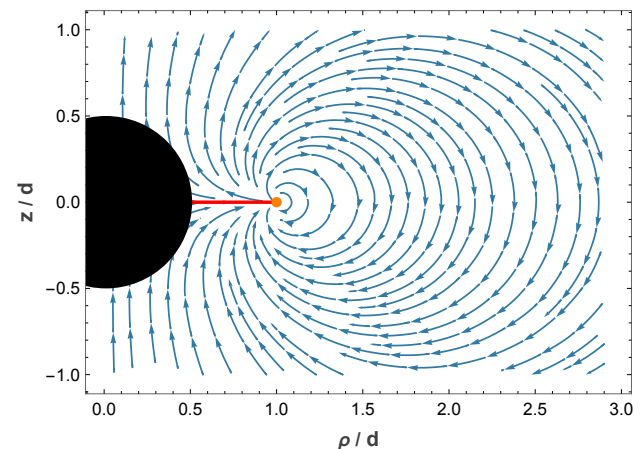
$$\lim_{d \rightarrow 0} v_1 = \sqrt{z^2 + \rho^2} - z, \quad \lim_{d \rightarrow 0} v_2 = \frac{\rho^2}{(z^2 + \rho^2)^{3/2}}. \quad (43)$$

These behaviors are evident in Fig. 1 by eyeballing. From these plots, the feature of the limiting curve as $d \rightarrow \infty$, the external quadrupole field, is most apparent near the axis of symmetry whereas the structure of the limiting curve as $d \rightarrow 0$ becomes more prominent far from the axis. This happens because, in $\rho \ll d$ region, d can be treated as large compared to the local distance, whereas in the region $\rho \gg d$, d can be treated as very small. For the same reason, the two solutions exhibit asymptotically parabolic and dipolar behavior at infinity, respectively. Hence, we refer to these solutions as the *asymptotically parabolic* and the *asymptotically dipolar* solution in the remainder of the discussion.

In addition, in the limit $d \rightarrow \infty$, the two transformations given in Eqs. (38) and (39) correctly reduce to the



(a) asymptotically parabolic



(b) asymptotically dipolar

FIG. 1. Poloidal field lines corresponding to (a) asymptotically parabolic and (b) asymptotically dipolar around a compact object (black-filled region). The solid red lines represents the thin disk, and the small orange circle marks the location of current concentration.

appropriate transformation relating the vertical field, the asymptotic behavior of the hyperbolic solution, to the X-point solution,

$$\lim_{d \rightarrow \infty} L_1 = \lim_{d \rightarrow \infty} L_2 = -\frac{\rho}{2z}. \quad (44)$$

Likewise, as $d \rightarrow 0$, the two transformations correctly reduce to the transformation from the radial field, which corresponds to the limiting field of the hyperbolic solution, to the respective limits of the solutions: from radial to parabolic,

$$\lim_{d \rightarrow 0} L_1 = \frac{\sqrt{z^2 + \rho^2} - z}{\rho}, \quad (45)$$

and from radial to dipolar,

$$\lim_{d \rightarrow 0} L_2 = -\frac{\rho}{2z}. \quad (46)$$

These transformations are reported in Appendix A.

⁵ This field describes a magnetic null point.

B. Source of the vacuum fields

Each solution is sourced by a current sheet at the equatorial plane, with an apparent singularity at $\rho = d$. In both cases, the pullback of F to the plane is continuous, which implies the absence of magnetic monopoles. For the asymptotically parabolic solution, the surface current is given by

$$J = [\mathcal{J}_1 H(\rho - d) + \mathcal{J}_2 H(d - \rho)] \delta(z) dz \wedge d\rho \wedge dt, \quad (47a)$$

$$\mathcal{J}_1 = -\frac{(\psi_0/\pi)}{\rho}, \quad \mathcal{J}_2 = \frac{(\psi_0/\pi)\rho}{d^2 - \rho^2 + d\sqrt{d^2 - \rho^2}}, \quad (47b)$$

where $\delta(x)$ is the Dirac delta function and $H(x)$ is the Heaviside function (equals to one for $x > 0$ and vanishes for $x < 0$). It implies two discontinuous surface currents in the disk that behave differently: an inner current density,

$$\vec{J}_{\text{inner}} = -\frac{(\psi_0/\pi)\rho}{d^2 - \rho^2 + d\sqrt{d^2 - \rho^2}} \delta(z) H(d - \rho) \hat{\varphi}, \quad (48)$$

and an oppositely flowing outer current,

$$\vec{J}_{\text{outer}} = \frac{(\psi_0/\pi)}{\rho} \delta(z) H(\rho - b) \hat{\varphi}, \quad (49)$$

that are separated by a diverging current density at $\rho = d$ from the inner current. The divergence exhibits only an inverse square-root dependence on the separation distance, which is milder than the inverse-distance singularity characteristic of a line current. We can find that the total current integrated over the disk is finite. The same behavior applies to the magnetic field. Thus, while the disk contains a localized concentration of current at $\rho = d$, this concentration is weaker than that associated with a line current.

On the other hand, in the asymptotically dipolar solution, there is no outer disk extending beyond $\rho = d$, but a diverging current density is also present at the ‘outer’ disk edge $\rho = d$. The divergence grows inversely with $\sim (d^2 - \rho^2)^{3/2}$, faster than the divergence associated with a line current. It is unsurprising because $\rho = d$ is a caustic of magnetic field lines, which is visible in Fig. 1b. Consequently, the total current diverges, rendering this solution nonphysical.

In both cases, the parameter d does not represent an inner disk radius, as in the hyperbolic solution. One may redefine the solutions as $\psi' = \text{sgn}(z)\psi$, thereby restructuring the disk so that d can be interpreted as an inner disk radius. However, this modification introduces magnetic monopoles on the disk, which is undesirable.

Moreover, in both solutions, the magnetic fields that cross the compact object, surrounded by the disk, nontangentially intersect its surface twice (except for the last magnetic field touching the object). The double crossing of field lines on the surface and the divergence of the current density can be avoided by remodeling the solutions

through a translation along the z -axis,

$$u(\rho, z) \rightarrow u'(\rho, z) = u(\rho, z + \text{sgn}(z)z'), \quad (50)$$

by an amount z' greater than the radius of the object, and by gluing the solutions together at $z = 0$. The solutions are still force-free because the flat spacetime stream equation admits translational symmetry along z -axis in general. However, this construction may not correspond to an exact solution in Kerr spacetime and somewhat artificial, even perturbative solution is still possible, since the stream equation in Kerr spacetime lacks such translational symmetry. If one nevertheless insists on such a solution exists in Kerr spacetime, the field is sourced by a continuous disk extending from the horizon and vanishes at infinity. But we only consider in this paper the unmodified solution in which there is a concentration of current in the disk.

IV. BLACK HOLE FORCE-FREE JET

In the black hole magnetosphere, magnetic fields are only tied to the horizon, or rather the so-called stretched horizon, when viewed through the membrane paradigm. This horizon membrane acts like a unipolar inductor with finite resistance. For this reason, if the black hole is treated as the central object in our new force-free solution, field lines that would otherwise cross the surface—here, the horizon—twice become segmented into two causally disconnected parts. The open field lines that extend to infinity constitute the black hole jet, while the closed field lines that connect to the magnetized disk allow for the energy exchange between the black hole and the disk. Such black hole-disk field lines are featured in numerical solutions [23, 24], and their possible physical realization has been proposed in the magnetosphere of a rotating black hole surrounded by a magnetized accretion torus [25]. Both types of field lines must obey the regularity condition at the horizon, but are subject to different conditions at their other ends, and therefore rotate differently. However, in this paper, we focus exclusively on the properties of the black hole jet. The jet solution is obtained by promoting the solution in flat spacetime to Schwarzschild background and performing a BZ perturbation, as discussed next.

Blandford and Znajek [10] introduced a perturbative method for solving the stream equation in the Kerr spacetime as an expansion in the black hole spin parameter a . The method begins by considering a vacuum degenerate field in Schwarzschild spacetime, with a given flux function $\psi = X(r, \theta)$. In linear order, one then constructs a force-free field with the same flux function, and with angular velocity and current given by

$$\Omega_F = \frac{a}{M^2} W(X), \quad (51)$$

$$I = \frac{a}{M^2} Y(X), \quad (52)$$

where Y, W are independent of the black hole spin. This field, with any functions of Y and W , is force-free to first order in the black hole spin, $\mathcal{O}(a)$. But, this leaves us infinite degrees of freedom in Y and W .

To obtain the unique solution, two appropriate equations relating the three functions are needed to fix Y and W . These equations are provided by the regularity condition on the future horizon of the black hole r_H , and, in jet cases, by condition imposed at infinity. The functions Y and W are then fixed by $I_{r_H} = I_\infty$ throughout the entire jet, since the total current enclosed by a poloidal loop is always conserved in a force-free environment.

The first equation is provided by the Znajek condition [12],

$$I = (\Omega_F - \Omega_H) \sin \theta \partial_\theta \psi \quad \text{at } r = r_H, \quad (53)$$

which is a universal relation that always hold on the black hole future horizon. Here, Ω_H is the angular velocity of the black hole horizon, which can be approximated as $\Omega_H = a/(4M^2)$. This condition arises from the regularity requirement of the field at the horizon.

On the other hand, there is no universal relation that can be imposed at infinity, or at any other point in space, that, together with the Znajek condition, uniquely fixes the functions. Hence, one is still left with an extremely large class of solutions, which may not correspond to a family of exact solutions in Kerr spacetime, as pointed out in Ref. [16]. In the original BZ approach, this issue is addressed from a postulate concerning the relationship among the three functions at infinity. It assumes that the asymptotic behavior of the perturbative solution at large r follows the behavior of the rotating solution of the flux function in flat spacetime, since Kerr spacetime becomes approximately flat in this limit. This postulate, however, requires ψ to admit a rotating counterpart in flat spacetime, even though the current and angular velocity in the perturbation are constructed as spin-induced quantities. Moreover, it can lead to inconsistencies, as observed, for example, in the split-monopole field solution, where extending the perturbation to higher order in spin under the same assumption gives inconsistent large- r behavior [17].

There are mathematically consistent procedures for determining the appropriate conditions to impose at infinity for different flux functions, and without requiring rotating counterparts in flat spacetime. Grignani, Harmark, and Orselli [18] studied different types of asymptotics at infinity when the field is very close to the rotation axis in Kerr spacetime under the BZ expansion, where the force-free approximation is most reliable. In particular, they identified monopole-type, parabolic-type, and vertical-type asymptotics. They showed that asymptotically monopole solutions contain higher-order terms that are not well-behaved at infinity when the standard BZ perturbation scheme is applied. A consistent expansion in the spin parameter can be achieved by allowing logarithmic contributions in a within the perturbation [26]. So, the hyperbolic solution in [16], which is

asymptotically monopolar, may result to inconsistencies in higher-order terms under the BZ expansion. This issue does not arise for asymptotically parabolic fields under the BZ perturbation, provided that the condition

$$I = \pm 2\Omega_F \psi \quad \text{at } r \rightarrow \infty \quad (54)$$

is met. For asymptotically vertical fields, the BZ expansion remains valid without requiring any such condition; hence, a separate analysis is needed to determine the appropriate asymptotic behavior for this class of solutions to fix the current and angular velocity. To date, no similar analysis has been carried out in the literature for BZ perturbation of an asymptotically dipolar field.

In Sec. III, we found two vacuum solutions in flat spacetime that may be promoted to Schwarzschild spacetime and may then serve as seed solutions for BZ perturbation. But only the asymptotically parabolic solution is viable as a physically valid solution in the Kerr spacetime. As mentioned in Sec. III, the asymptotically dipolar solution has a caustic of magnetic field lines in flat spacetime located at the outer edge of the disk, which cannot be removed in the Kerr background. Because of this feature, the total current throughout the disk diverges and all the magnetic field lines corotate with the outer edge of the disk, and thus the Znajek condition cannot also be satisfied by the magnetic fields threading the horizon in the black hole case. Moreover, a rotating black hole cannot sustain a magnetosphere consisting entirely of closed magnetic field lines sourced by an accretion disk, due to the strong twisting of the field lines, and the jet formation naturally involves open field lines [23, 27, 28]. As a result, the poloidal structure of a dipolar field in a nonrotating background cannot, in principle, be sustained around a rotating black hole, and thus the BZ perturbation cannot be performed consistently. For these reasons, we focus only on the asymptotically parabolic solution to model a black hole jet in this paper and investigate its properties. Also, in what follows, our analysis is confined to the northern hemisphere, $0 \leq \theta \leq \pi/2$, since the fields in the southern hemisphere can be recovered by reflection.

A. Magnetic flux function

To promote the asymptotically parabolic solution in flat background to Schwarzschild spacetime, we first perform a mode expansion of Eq. (40) around $r = 0$ and $r = \infty$. The resulting expansions are the following:

$$\psi_{\text{flat}}^<(r, \theta) = \frac{r}{\sqrt{\pi}} \sum_{k=1}^{\infty} \frac{\Gamma(k + \frac{1}{2})}{\Gamma(k + 1)} \left(\frac{r}{d}\right)^{2k} \Theta_{2k}(\theta), \quad (55)$$

$$\psi_{\text{flat}}^>(r, \theta) = r(1 - \cos \theta) - \frac{d}{2\sqrt{\pi}} \sum_{k=1}^{\infty} \frac{\Gamma(k - \frac{1}{2})}{\Gamma(k + 1)} \left(\frac{d}{r}\right)^{2k-1} \Theta_{2k-1}(\theta), \quad (56)$$

where we set $\psi_0 = 1$ in the meantime. Both series in the two expansions have a common radius of converge d , the location of the current concentration. Hence, $\psi_{\text{flat}}^<$ is valid only in $r \leq d$, while $\psi_{\text{flat}}^>$ is valid in $r \geq d$. It can be verified that these solutions agree on $r = d$, where they are equal to $d(\sqrt{\cos\theta} - \cos\theta)$. Also, in these expansions, the asymptotically parabolic behavior of the solution becomes evident.

As discussed in Sec. II, each mode in the expansions can be promoted to Schwarzschild spacetime by sending $r^{2k+1} \rightarrow R_{2k}^<(r)$ and $r^{-(2k-1)} \rightarrow R_{2k-1}^>(r)$ in the summations of Eqs. (55) and (56), respectively, and by allowing a relative normalization C for the inner solution. In doing so, the radius of convergence of both summations changes to

$$d_o = d + M + \frac{M^2}{4d}, \quad (57)$$

which is now the location of the sign-reversal of the current disk and current concentration in the Schwarzschild solution (see Appendix B).

The flux function vanishes at the location of the current concentration in the disk in flat spacetime. Upon promoting the inner solution to Schwarzschild spacetime, the flux function continues to vanish at the location of the current concentration, as expected. However, the leading term in the outer solution (56) becomes $r + 2M \log(1 - r/2M)$ if one attempts the mapping $r \rightarrow R_0^<(r)$, which is a solution of the $l = 0$ radial equation. With this term, the whole outer solution does not vanish at the location of the current concentration. To address this issue, we determine the general solution of the $l = 0$ radial equation. The constants of integration are then fixed by requiring the full outer flux function to vanish at the location of the current concentration, and by requiring the solution to reduce to r when $M = 0$ or as $r \rightarrow \infty$. The $\log(r - 2M)$ term in the solution does not pose a problem for the outer solution, provided that the location of the current concentration lies away from the horizon. The inner and outer solutions are given in the Appendix B.

B. Current and angular velocity

To implement the BZ perturbation, only the near-horizon behavior of the solution is required. From Eqs. (B1), this behavior is

$$X(r = r_H, \theta) \approx \alpha X_H \cos\theta \sin^2\theta, \quad (58)$$

where

$$X_H = \frac{16 C X_0 M^3}{\alpha \left[d_o - M + \sqrt{d_o(d_o - 2M)} \right]^2} \quad (59)$$

is the total magnetic flux of the jet on the horizon, balanced by a negative flux associated with black hole-disk

field lines, such that the total magnetic flux on one hemisphere of the horizon vanishes. Here, X_0 is a constant representing the total magnetic flux per unit radial distance in one hemisphere at large r , and

$$\alpha = \csc^2 \theta_o \sec \theta_o \quad (60)$$

is a constant determined by the angle θ_o at which the last field line touches the horizon. This angle can be determined from the condition that $\partial_\theta \psi = 0$ at the horizon.

In the flat spacetime solution, the last field line touches a central object with radius R at the angle

$$\theta_o^{\text{flat}} = \arctan \sqrt{\frac{2l^6 + 2l^4 - 6l^2 + 1 + \sqrt{9 - 8l^2}}{2(1 - l^2)^3}}, \quad (61)$$

where we define $l \equiv R/d$ and write the radicand in a form that explicitly requires $0 \leq l < 1$. In an external quadrupole field, the angle at which the last field line touches the surface is exactly $\arctan(\sqrt{2})$, or about 54.7° . For our solution, in the large- d limit, the angle is

$$\theta_o^{\text{flat}} = \arctan(\sqrt{2}) + \mathcal{O}(l^2). \quad (62)$$

The correction appears at second order in l and higher. We expect that, in Schwarzschild background, the correction due to the black hole appears at the same order in r_H/d_o in the limit $d_o \gg r_H$. Thus, we may approximate $\theta_o \simeq \arctan(\sqrt{2})$ in Eq. (60) in the large- d_o limit.

However, the location at which the reversal of the disk current and the current concentration is most likely to happen is not far from the horizon, due to dynamics between the strong gravitational and electromagnetic forces to the plasma in this region. Such an interaction may also be the reason a current disk persist inside the innermost stable circular orbit (ISCO). This behavior is observed in several analyses, such as studies of magnetically arrested disks (MADs), where the inflow of the magnetized accreting matter is halted because of the concentration of magnetic field, and magnetic reconnection [29, 30]. Hence, although results in the large- d_o limit are analytically tractable and reliable, it is also necessary to consider the small- d_o regime.

Finding the exact value of θ_o in the small- d_o case appears intractable, as can be seen from Eq. (B1). Nevertheless, we may assume that the angle does not differ significantly from that given in Eq. (61), with l being replaced by r_H/d_o , so that θ_o reduces to the flat spacetime value when the mass is ‘‘scooped out’’ of the black hole at the same radius. In the limit $d_o \rightarrow \infty$, we obtain $\theta_o = \arctan \sqrt{2}$, in agreement with our previous assumption. Also, the last jet field line is anchored to the disk. Hence, we expect the flux function of the last field line to remain close to its flat spacetime counterpart when d_o is not too close to the horizon, which in turn implies that θ_o is close to θ_o^{flat} in this case. A large deviation would otherwise imply that the black hole significantly alters the structure of the last field line in the region where the gravitational effect should be small. For instance, when

d_o is at the ISCO radius, $r = 6M$, the last field line angle according to our approximation is $\theta_o \approx 56.5^\circ$, and the flat spacetime counterpart is $\theta_o^{\text{flat}} \approx 57.4^\circ$. This approximation, however, breaks down when d_o lies very close to the horizon, where the effects of the strong gravitational field become significant along the entire last jet field line.

We can use Eq. (58) to treat the angle at the horizon θ_H as a parameter labeling the field lines,

$$\theta_H(x) = \arccos \left\{ \frac{2}{\sqrt{3}} \cos \left[\frac{1}{3} \arccos \left(-\frac{3\sqrt{3}x}{2\alpha} \right) \right] \right\}, \quad (63)$$

where $x \equiv X/X_H$. Then, the Znajek horizon condition requires

$$Y = \frac{\alpha}{2} X_H \left(W - \frac{1}{4} \right) [1 + 3 \cos(2\theta_H)] \sin^2(\theta_H). \quad (64)$$

Meanwhile, we use the condition in Eq. (54) at infinity,

$$Y = -2WX, \quad (65)$$

with the choice of sign as the appropriate sign to describe energy extraction by the jet. By equating Eqs. (64) and (65), we find the angular velocity as

$$W = \frac{1}{4} - \frac{x}{4x + \alpha[1 + 3 \cos(2\theta_H)] \sin^2 \theta_H}. \quad (66)$$

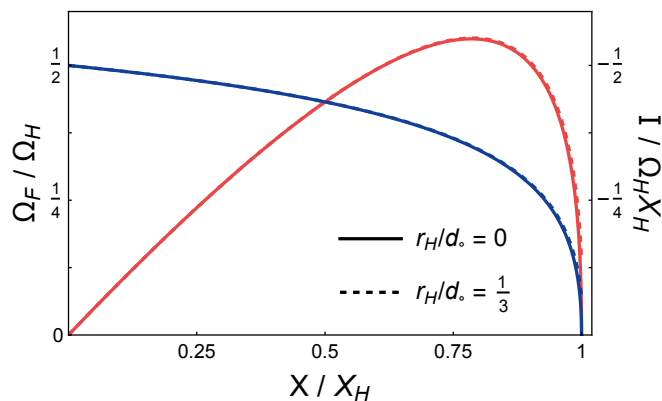


FIG. 2. Angular velocity (blue) and current (red) of the field lines for $d_o = r_{\text{ISCO}}$ (dashed lines) and $d_o \rightarrow \infty$ (solid lines) as functions of X/X_H . The angular velocity and current are insensitive to d_o .

By judging Eq. (66), the jet field lines attain their maximum angular velocity along the rotation axis, equal to half of the horizon angular velocity, and the angular velocity then decreases monotonically toward the last field line. This angular velocity profile is evident in the cases we consider, $d_o = r_{\text{ISCO}} = 6M$ and $d_o \rightarrow \infty$, as shown in Fig. 2. Also, we may infer from the figure that, within this d_o domain, the current and angular velocity are largely insensitive to d_o for the bulk of the jet, with minimal differences appearing only near the boundary

of the jet, at fixed X_H . The reason of this insensitivity is because $\theta_o(d_o \rightarrow \infty) \approx \theta_o(d_o = r_{\text{ISCO}})$ leading to $\alpha(d_o \rightarrow \infty) \approx \alpha(d_o = r_{\text{ISCO}}) \approx 2.6$. Although we are limited by our expression for θ_o , it is also possible that this insensitivity persists even when $d_o < r_{\text{ISCO}}$.

A difference arises for the last jet field line. The angular velocity of the last field line vanishes as $d_o \rightarrow \infty$, whereas it takes a nonzero value for $d_o = r_{\text{ISCO}}$; a similar behavior is observed in the current. This difference is largely a consequence of our approximation. In fact, the last field line is expected to have zero angular velocity and current for any value of d_o because its $\partial_\theta \psi$ vanishes at the horizon, which, together with the horizon regularity condition and the condition at infinity, implies this behavior. Since the last field line is also tied to a current in the disk, it should not corotate with the current. Instead, the field line must be slipping through the current, or the current must possess a finite resistance, in order to account for the vanishing of its angular velocity.

In addition, the last jet field line has adjacent field lines: one anchored in the disk and extending to infinity, and another anchored in the disk and connected to the black hole. The field line anchored in the disk and extending to infinity may constitute the disk wind. Since the current and angular velocity of the last field line do vanish for any d_o , and since a boundary condition at infinity cannot be imposed on the disk-wind field line, a current sheet may possibly form between the jet and the wind. Meanwhile, there may exist, in principle, a transition region extending from the horizon to the current at which the last jet field line is slipping through, within which the angular velocity and current changes smoothly to zero. Moreover, the current along the black hole-disk field lines flows opposite to that of the jet field lines. This reversal arises because $\partial_\theta \psi$ of the hole-disk field lines changes sign, implying that energy flow from the disk to the black hole, as expected on physical grounds. But, whether the black hole-disk system as a whole results in net energy extraction depends on the properties of the hole-disk field lines and, ultimately, by the properties of the disk.

C. Jet power and circuit model

The Blandford–Znajek mechanism enables the extraction of energy from a rotating black hole by a force-free field, providing an explanation for the release of black hole electromagnetic jets. Specifically, a stationary axisymmetric force-free field around a black hole admits Noether currents associated with its symmetries [20]. Time-translation symmetry corresponds to the *Killing energy* (i.e., the energy measured at infinity), while azimuthal-translation symmetry corresponds to the *Killing angular momentum*. The Killing energy and angular momentum are conserved as they propagate along the poloidal field lines. For a local observer, the Killing energy is interpreted as spatial angular momentum in the ergoregion. Hence, a negative energy flux can

flow into the black hole from the ergoregion while being balanced by a positive energy flux to infinity. The power extracted by this mechanism is given by

$$\mathcal{P} = -\frac{1}{2\pi} \int I(\psi), \Omega_F, d\psi. \quad (67)$$

We find that, in the large d_o -limit and for the $d_o = r_{\text{ISCO}}$, the extracted power is approximately the same,

$$\mathcal{P} \approx 2.2 \times 10^{-2} X_H^2 \Omega_H^2. \quad (68)$$

We note that this expression for the power accounts only for the jet in the northern hemisphere. This power is also comparable to the energy output of the hyperbolic jet at fixed horizon magnetic flux and angular velocity. The near equality of the power, which is also observed for the hyperbolic jet [16], arises from the weak dependence of the angular velocity and the current on d_o . In general, however, the power differs significantly for different values of d_o once the condition of fixed X_H is relaxed, since X_H depends on the disk. In particular, at finite X_0 , the horizon magnetic flux becomes very small in the large d_o , and the power correspondingly becomes insignificant too. This behavior is physically reasonable, as the disk sourcing the strong magnetic field is then very far from the black hole. But, regardless of the profile of the disk, the power in (68) shows a clear interpretation of the Blandford-Znajek mechanism as an energy-extraction process on the horizon, in which the extracted power depends solely on the amount of field lines threading the horizon and the horizon angular velocity.

Also, the other importance of our analysis at fixed X_H lies in determining the effective resistance of the jet when it is modeled as a circuit with the load at infinity. This quantity is independent of the horizon magnetic flux and therefore provides a characterization of the jet that remains approximately valid for any value of d_o . The voltage drop along a field line is given by the integral of $\Omega(\psi) d\psi$. For large d_o , the net current increases from zero to a maximum at $X/X_H \approx 0.785$, and then decreases to zero at the boundary of the jet. We may regard $X \lesssim 0.785 X_H$ as the flow of forward current in the bulk of the jet and $X \gtrsim 0.785 X_H$ as the return flow of current. The corresponding approximate bulk current of the jet is

$$I(0.785 X_H) = I_{\text{bulk}} \approx -0.55 X_H \Omega_H, \quad (69)$$

and the voltage drop across the jet is

$$\begin{aligned} V &= 4 X_H \Omega_H \int_0^1 W\left(x; \alpha = \frac{3\sqrt{3}}{2}\right) dx \\ &\approx 0.405 X_H \Omega_H. \end{aligned} \quad (70)$$

Then, the effective resistance is

$$R_{\text{eff}} = \frac{V}{|I_{\text{bulk}}|} \approx 0.74. \quad (71)$$

Since we find that the jet properties depend only weakly on d_o , this approximate value holds for any d_o . The effective resistance of our black hole jet is comparable to that of the black hole hyperbolic jet, greater than that of the stellar hyperbolic jet (see Ref. [16]). Hence, our new analytic jet solution is consistent with the intuition of the membrane paradigm that black hole horizon provides additional effective resistance, as suggested by comparison with the stellar hyperbolic jet, although a stellar counterpart of our solution is not presented here.

V. SUMMARY AND OUTLOOK

With the advances in our understanding of the geometric spacetime structure of force-free fields, we now have new tools and perspectives to search for new analytic solutions to force-free electrodynamics beyond the conventional methods.

In this work, we combined this innovation with previous methods to construct a new analytic jet model from a disk-fed rotating black hole. First, we found new parametrized vacuum solutions in flat spacetime by applying the geometric procedure developed in [13] to a hyperbolic solution. Among these solutions, we identify one that is physically viable and of particular interest, while the other is deemed unphysical; we reported the ‘unphysical’ solution anyway for its potential application to stellar magnetospheres. Then, we extended the physical solution to Schwarzschild spacetime and seeded it into the Blandford-Znajek perturbative method, in an equivalent fashion to the construction of the black hole hyperbolic jet [16]. Thus, our jet model constitutes a perturbative analytic solution.

Our black hole jet exhibits a radially varying structure, transitioning from a magnetic null field structure near the horizon to an asymptotically parabolic configuration at large distances. This variability is of interest, given that the observed jet boundary of M87* displays approximately, rather than genuine, parabolic geometry at $\sim 10^1 - 10^5$ gravitational radius [31]. It would be worthwhile to assess the jet boundary geometry in future work.

The global magnetosphere in our model corresponds to a black hole-disk system in which the thin equatorial disk contains a coincident current sign reversal and current concentration, and sources the magnetic field. The poloidal field lines extending to infinity from the horizon constitute the jet, while other field lines thread the horizon and are anchored to the disk, allowing energy transport from the disk to the black hole. Also, field lines beyond the jet remain anchored to the disk and may contribute to magnetized disk wind, suggesting the possible formation of a current sheet at the jet boundary.

Moreover, the location of the current concentration and sign reversal parametrizes the flux function of our black hole jet, and so the total poloidal current and angular velocity. But, the jet properties are insensitive to this

parameter at fixed horizon angular velocity and magnetic flux. Hence, we obtain a jet power given in Eq. (68) that is valid for any value of the parameter within the approximation. This situation is similar to that of the hyperbolic jet. In both the hyperbolic and our new asymptotically parabolic jets, the insensitivity to the disk parameter extends not only to the jet power but also to the entire jet properties, although this aspect of the hyperbolic jet has not been emphasized in previous literature [16]. It would be interesting to investigate, however, whether the apparent insensitivity of the jets reflects a genuine independence of the jets properties from the disk parameter and an artifact of the approximations used.

These results illustrate the standard interpretation that the Blandford-Znajek mechanism operates as an energy-extraction process on the horizon, independent of the source of the magnetic field. By examining the jet power derived here, together with those of other jets from disk-fed black holes, one finds that all jet powers depend only on the magnetic flux threading the horizon and the horizon angular velocity, and not on the detailed properties of the disk - a feature expected from the BZ process. The question of whether this process should be understood as being mediated by the horizon through the membrane paradigm or by the ergosphere has been extensively debated. But numerical simulations favor the latter interpretation [32, 33].

In addition, the effective resistance of the jet, when compared with that of a known stellar jet, is compatible with the membrane paradigm notion that the horizon possesses a finite resistance. It is also comparable to the effective resistance found in the black hole hyperbolic jet.

Appendix A: Rotation in vacuum tetrad

Suppose we have a spherically symmetric spacetime background,

$$ds^2 = -g_{tt}dt^2 + g_{rr}dr^2 + r^2d\theta^2 + r^2\sin^2\theta d\varphi^2. \quad (\text{A1})$$

A vacuum degenerate field can always be written as

$$F = h d\hat{\psi} \wedge \omega, \quad h \equiv \frac{\|d\psi\|}{r \sin\theta}, \quad (\text{A2})$$

where $d\hat{\psi} \equiv d\psi/\|d\psi\|$ and $\omega \equiv (r \sin\theta d\varphi)$. The flux function depends only on the poloidal coordinates (r, θ) , so $d\hat{\psi}$ lies on the poloidal subspace that is constant along the integral curves of the Killing fields ∂_t and ∂_φ , and it is orthogonal to ω . In contrast, ω lies on the toroidal subspace generated by the Killing fields with coordinates (t, φ) .

Using the identity for the dual of a p -form constructed from orthogonal forms (see Appendix 2.2 of Ref. [20]), the dual field is

$$*F = hv \wedge \rho, \quad (\text{A3})$$

where $v \equiv -\sqrt{g_{tt}}dt$ and $\rho \equiv \star d\hat{\psi}/\sqrt{g_{tt}}$, with \star denoting the dual taken with respect to the poloidal subspace. These one-forms, $v, \rho, d\hat{\psi}, \omega$, make a tetrad in the background spacetime. Thus, we can assign them as $e_0^b, e_1^b, e_2^b, e_3^b$, respectively. Being a degenerate Maxwell field means that e_0 and e_1 forms an involutive distribution.

Notably, v and ω depend only on the background geometry and not on the magnetic flux function. Then, e_0^b and e_1^b are always the same for a vacuum field on a fixed background spacetime. Hence, any tetrad associated with a vacuum field and transformed by a homogeneous Lorentz transformation satisfies

$$\bar{e}_0 = \Lambda_0^a e_a = e_0, \quad \bar{e}_3 = \Lambda_3^a e_a = e_3, \quad (\text{A4})$$

which implies that

$$\delta_{ij}\Lambda^j_0 = \delta_{i0}, \quad \delta_{ij}\Lambda^j_3 = \delta_{i3}, \quad (\text{A5})$$

where δ_{ij} is the Kronecker delta. Moreover, with this condition and the similarity transformation $\Lambda^T \eta \Lambda = \eta$, we also have

$$\delta^{ij}\Lambda^0_j = \delta^{i0}, \quad \delta^{ij}\Lambda^3_j = \delta^{i3}, \quad (\text{A6})$$

and

$$\delta_{kl}\Lambda^k_m \Lambda^l_{m'} = \delta_{mm'}, \quad (\text{A7})$$

with $k, l, m, m' = 1, 2$. But this is exactly the definition of orthogonal transformation on e_1 - e_2 plane, or on the poloidal plane. For instance, the vertical, X-point, radial, parabolic and dipolar fields have the following respective tetrad bases:

$$\text{All fields: } \begin{aligned} e_0 &= \partial_t \\ e_3 &= \frac{1}{\rho} \partial_\varphi \end{aligned}, \quad (\text{A8})$$

$$\text{Vertical: } \begin{aligned} e_1 &= -\partial_z \\ e_2 &= \partial_\rho \end{aligned}, \quad (\text{A9})$$

$$\text{X-point: } \begin{aligned} e_1 &= \frac{\rho}{\sqrt{4z^2 + \rho^2}} \partial_\rho - \frac{2z}{\sqrt{4z^2 + \rho^2}} \partial_z \\ e_2 &= \frac{\rho}{\sqrt{4z^2 + \rho^2}} \partial_z + \frac{2z}{\sqrt{4z^2 + \rho^2}} \partial_\rho \end{aligned}, \quad (\text{A10})$$

$$\text{Radial: } \begin{aligned} e_1 &= -\frac{z}{\sqrt{z^2 + \rho^2}} dz - \frac{\rho}{\sqrt{z^2 + \rho^2}} \partial_\rho \\ e_2 &= -\frac{\rho}{\sqrt{z^2 + \rho^2}} \partial_z + \frac{z}{\sqrt{z^2 + \rho^2}} \partial_\rho \end{aligned}, \quad (\text{A11})$$

$$\text{Parabolic: } \begin{aligned} e_1 &= \frac{[(z - \sqrt{z^2 + \rho^2}) \partial_\rho - \rho \partial_z]}{\sqrt{2(z^2 + \rho^2 - z\sqrt{z^2 + \rho^2})}} \\ e_2 &= \frac{[(z - \sqrt{z^2 + \rho^2}) \partial_z + \rho \partial_\rho]}{\sqrt{2(z^2 + \rho^2 - z\sqrt{z^2 + \rho^2})}} \end{aligned}, \quad (\text{A12})$$

$$\text{Dipolar : } \begin{aligned} e_1 &= \frac{[(\rho^2 - 2z^2)\partial_z - 3z\rho\partial_\rho]}{\sqrt{(z^2 + \rho^2)(4z^2 + \rho^2)}} \\ e_2 &= \frac{[-3z\rho\partial_z + (2z^2 - \rho^2)\partial_\rho]}{\sqrt{(z^2 + \rho^2)(4z^2 + \rho^2)}} \end{aligned} \quad (\text{A13})$$

With these tetrads, it can easily be shown that applying the transformation in Eq. (34) with $L = \rho/2z$ to the vertical tetrad gives the X-point tetrad. In similar transformation, the radial tetrad transforms into parabolic and dipolar tetrads for $L = (\sqrt{z^2 + \rho^2} - z)/\rho$ and $L = -\rho/2z$, respectively. We find that all vacuum solutions in Ref. [22] are related through this connection.

Appendix B: Normalization and radius of convergence of Schwarzschild solution

The promoted inner and outer solutions in Schwarzschild spacetime referred to in Sec. IV are given by

$$\psi^<(r, \theta) = \frac{C}{\sqrt{\pi}} \sum_{k=1}^{\infty} \frac{\Gamma(k + \frac{1}{2})}{\Gamma(k + 1)} \frac{R_{2k}^<(r)}{d^{2k}} \Theta_{2k}(\theta), \quad (\text{B1})$$

$$\begin{aligned} \psi^>(r, \theta) &= \left[r - d_o + 2M \log\left(\frac{r - 2M}{d_o - 2M}\right) \right. \\ &+ \frac{1}{2\sqrt{\pi}} \sum_{k=1}^{\infty} \frac{\Gamma(k - \frac{1}{2})}{\Gamma(k + 1)} d^{2k} R_{2k-1}^>(d_o) \left. \right] (1 - \cos \theta) \\ &- \frac{1}{2\sqrt{\pi}} \sum_{k=1}^{\infty} \frac{\Gamma(k - \frac{1}{2})}{\Gamma(k + 1)} d^{2k} R_{2k-1}^>(r) \Theta_{2k-1}(\theta), \quad (\text{B2}) \end{aligned}$$

with $d_o > 2M$. As mentioned in Ref. [16], the series involved in any promoted inner and outer solutions are expected to match because of the unique, well-defined correspondence between the solutions in the flat and Schwarzschild spacetimes. But, in the promotion we employed, the association acts only on local neighborhood of the exact global solution up to an undetermined overall constant. As a consequence, promoting any flat spacetime solution in this way leaves a relative normalization between the ‘local’ promoted solutions.

In addition, the matching of the inner and outer solutions at the same radius of convergence d_o , for all the angles can be assessed only numerically. In particular, we

can check that the solutions match at d_o using the expression for C derived from the angle $\theta = \pi/4$ in this section. A definitive numerical verification is hindered, however, by the slow convergence of the series for any angle. In fact, the series falls only like $k^{-3/2}$ for $\theta = \pi/4$, and it requires $\sim 10^3$ summation terms to obtain a good accuracy. We have shown the matching of the two solutions, anyway, at a specific condition in Fig. 3 with reasonable precision. We have therefore relied on the presumed continuity of the solutions in any circumstances from this example, along with the qualitative verification of our expression of C at the end of this section.

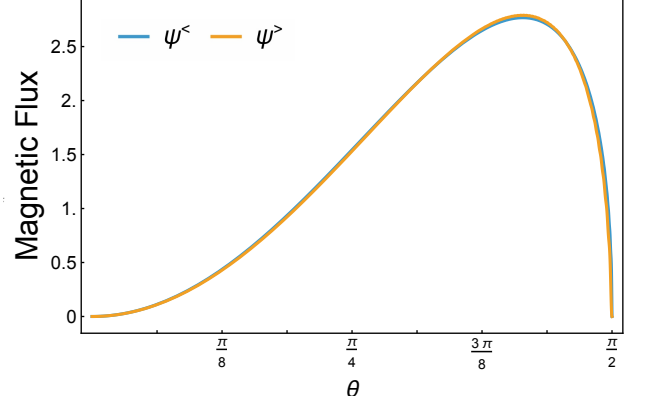


FIG. 3. Inner (blue) and outer (orange) magnetic flux evaluated at d_o for all the northern polar angles all using the same normalization C derived in Appendix B. We used $d_o = 6M$ and $M = 2$ in this plot.

In this section, we show that the common radius of convergence of the solutions, implied by the present summations, is d_o , and we derive an approximate expression for C . We do not derive the radius of convergence for the flat spacetime solution here, as it is obtained by taking the $M = 0$ limit of the result derived in this section. We also expect it to be equal to d , since the solutions were, from the outset, expansions inside and outside the radius d . Although this result can be proved analytically in a straightforward manner, we omit the proof in this section. Throughout this section, we make use of the asymptotic approximations of the hypergeometric function given on p. 77 of Ref. [34],

$$\begin{aligned} {}_2F_1[a + \lambda, a - c + 1 + \lambda; a - b + 1 + 2\lambda; 2(1 - z)^{-1}] &\stackrel{\lambda \rightarrow \infty}{\sim} 2^{a+b} \left(\frac{z-1}{2}\right)^{a+\lambda} \frac{\Gamma(a-b+1+2\lambda)\Gamma(\frac{1}{2})\lambda^{-1/2}}{\Gamma(a-c+1+\lambda)\Gamma(c-b+\lambda)} \\ &\times e^{-(a+\lambda)\xi} (1 - e^{-\xi})^{-c+\frac{1}{2}} (1 + e^{-\xi})^{c-a-b-\frac{1}{2}} [1 + \mathcal{O}(\lambda^{-1})], \quad (\text{B3}) \end{aligned}$$

$$\begin{aligned} {}_2F_1\left[a + \lambda, b - \lambda; c; \frac{1-z}{2}\right] &\stackrel{\lambda \rightarrow \infty}{\sim} \frac{\Gamma(1-b+\lambda)\Gamma(c)}{\Gamma(\frac{1}{2})\Gamma(c-b+\lambda)} 2^{a+b-1} (1 - e^{-\xi})^{-c+\frac{1}{2}} (1 + e^{-\xi})^{c-a-b-\frac{1}{2}} \lambda^{-\frac{1}{2}} \\ &\times [e^{(\lambda-b)\xi} + e^{\pm i\pi(c-1/2)} e^{-(\lambda+a)\xi}] [1 + \mathcal{O}(|\lambda^{-1}|)], \quad (\text{B4}) \end{aligned}$$

where ξ is defined by $e^\xi \equiv z + \sqrt{z^2 - 1}$, and the upper or lower sign is chosen according to whether $\text{Im}(z) \gtrless 0$. Equivalently, $e^{-\xi} = z - \sqrt{z^2 - 1}$. For real z arguments,

one may consider $z = a \pm i\epsilon$ and take $\epsilon \rightarrow 0$ that leaves a consistent result in the asymptotic expansion.

1. Radius of convergence

The asymptotic behavior of the odd- l angular solution as $k \rightarrow \infty$ is provided in Eq. (B27) of Gralla. The corresponding even- l angular solution is obtained by setting $a = 1/2$, $b = 0$, $c = 3/2$, $\lambda = k$, and $z = 1 - 2\cos^2\theta$ in Eq. (B4),

$$\theta_{2k}(\theta) \stackrel{k \rightarrow \infty}{\sim} -\frac{1}{2\sqrt{2k}} \frac{\Gamma(k+1)}{\Gamma(k+\frac{3}{2})} \frac{e^{i\theta} \sin\theta}{\sqrt{1-e^{2i\theta}}} [(-e^{-2i\theta})^{k+1/2} - (-e^{-2i\theta})^{-k}]. \quad (\text{B5})$$

This asymptotic expression of θ_{2k} is real at all θ , but it generally requires a careful cancellation of the complex phases. In addition, the asymptotic behavior of the even- l inner radial solution (30) in the same limit can be obtained by setting $a = 2$, $b = 1$, $\lambda = 2k$, $c = 3$, $z = 1 - r/M$ in Eq. (B4),

$$R_{2k}^<(r) \stackrel{k \rightarrow \infty}{\sim} \sqrt{\frac{8}{\pi k}} \frac{\Gamma(2k)\Gamma(2k+2)}{\Gamma(4k+1)} (2M)^{2k-1} r^2 \frac{(e^{-2k\xi} + ie^{(2k+1)\xi})}{(1-e^\xi)^2 \sqrt{e^{-2\xi} - 1}}, \quad e^\xi = 1 - \frac{r - \sqrt{r(r-2M)}}{M}, \quad (\text{B6})$$

where lower sign is chosen so that the real part of the radial function is always positive. Note that $0 < |e^\xi| < 1$ for $2M < r$; hence the imaginary part in Eq. (B6) virtually vanishes as $k \rightarrow \infty$. If we rewrite the inner solution as

$$\psi^<(r, \theta) = C \sum_{k=1}^{\infty} a_k^<, \quad a_k^< \equiv \frac{1}{\sqrt{\pi}} \frac{\Gamma(k+\frac{1}{2})}{\Gamma(k+1)} \frac{R_{2k}^<(r)}{d^{2k}} \Theta_{2k}(\theta), \quad (\text{B7})$$

the asymptotic behavior of the summation term, using Eqs. (B5) and (B6), is

$$a_k^< \stackrel{k \rightarrow \infty}{\sim} \frac{(-1)^k}{k\sqrt{\pi}} \frac{r^2}{2M} \frac{\Gamma(2k)}{\Gamma(2k+\frac{1}{2})} \left(\frac{M}{2d}\right)^{2k} \sqrt{\frac{1-e^{2i\theta}}{e^{-2\xi}-1}} \frac{(e^{-2k\xi} + ie^{(2k+1)\xi})(e^{-(2k+1)i\theta} + ie^{2ki\theta})}{(1-e^\xi)^2}. \quad (\text{B8})$$

In general, the ratio $|a_{k+1}^</a_k^<|$ wildly oscillates, and thus does not approach a smooth limit to perform the ratio test. But evaluating the summation term at $\theta = \pi/4$ allows the sum to be separated into even and odd k contributions as

$$\sum_{k=1}^{\infty} a_k^< = \sum_{m=1}^{\infty} a_{2m+1}^< + \sum_{n=1}^{\infty} a_{2n}^<, \quad (\text{B9})$$

due to the angular part

$$\Theta_{2k}(\theta = \pi/4) \stackrel{k \rightarrow \infty}{\sim} \frac{1}{4\sqrt{k}} \frac{\Gamma(k+1)}{\Gamma(k+\frac{3}{2})} \left[\sqrt{\sqrt{2}-1} \cos\left(\frac{k\pi}{2}\right) + \sqrt{\sqrt{2}+1} \sin\left(\frac{k\pi}{2}\right) \right], \quad (\text{B10})$$

from which we see that $|a_{k+2}^</a_k^<|$ does not oscillate wildly. Then, we may instead perform the ratio test on each contribution separately. We find that both contributions have the same ratio of consecutive terms in the limit $k \rightarrow \infty$,

$$L = \lim_{m \rightarrow \infty} \left| \frac{a_{2m+1}^<}{a_{2m-1}^<} \right| = \lim_{n \rightarrow \infty} \left| \frac{a_{2n+2}^<}{a_{2n}^<} \right| = \left(\frac{M}{2d}\right)^4 |e^{-4\xi}| = \left(\frac{M}{2d}\right)^4 \left[\frac{r + \sqrt{r(r-2M)}}{M} - 1 \right]^4, \quad (\text{B11})$$

Thus, by demanding that $L = 1$, we find

$$d = \frac{r - M + \sqrt{r(r-2M)}}{2}, \quad (\text{B12})$$

which gives the radius of convergence in Eq. (57), such that $L < 1$ for every $2M < r < d_\circ$. Alternatively, although all a_k 's are zero at $\theta = \pi/2$, we may first take the limit $\theta \rightarrow \pi/2$ of the ratio a_{k+1}/a_k and then perform the ratio test. This procedure yields the same radius of convergence.

For completeness, we also show that the outer solution has the same radius of convergence as the inner solution. The outer solution, on the other hand, has two summations, one of which arises from the $l = 0$ stream equation. This summation is simply the last term evaluated at $r = d_o$ and $\theta = \pi/2$. Thus, establishing convergence of the last summation at $\theta = \pi/2$, where the ratio of the consecutive terms does not fluctuate wildly, is sufficient to prove that $r = d_o$ is the radius of convergence of the full solution.

Since the asymptotic behavior of the odd- l angular solution is already known, we only need to show here the asymptotic expression for $R_{2k-1}^>(r)$. Applying the Pfaff transformation

$${}_2F_1[a, b; c; z] = (1-z)^{-a} {}_2F_1[a, c-b; c; z/(z-1)] \quad (\text{B13})$$

to the odd- l case in Eq. (32) gives

$$R_{2k-1}^>(r) = r^{-(2k-1)} \left(1 - \frac{2M}{r}\right)^{-(2k+1)} {}_2F_1\left[2k+1, 2k+1; 4k; \frac{1}{1-r/2M}\right]. \quad (\text{B14})$$

Then, with the choice of $a = 1$, $b = 2$, $c = 1$, $\lambda = 2k$, and $z = r/M - 1$ in Eq. (B3), the asymptotic expression for the odd- l outer solution is

$$R_{2k-1}^>(r) \stackrel{k \rightarrow \infty}{\sim} \sqrt{\frac{32\pi}{k}} \left(\frac{e^{-\xi}}{2M}\right)^{2k+1} \frac{\Gamma(4k)}{\Gamma(2k+1)\Gamma(2k-1)} \frac{r^2}{(1+e^{-\xi})^2 \sqrt{1-e^{-2\xi}}}, \quad (\text{B15})$$

where this time $0 < e^\xi < 1$ for $2M < r$. Rewriting the summation in the last term of the outer solution as

$$\sum_{k=1}^{\infty} \frac{\Gamma(k - \frac{1}{2})}{\Gamma(k+1)} d^{2k} R_{2k-1}^>(r) \Theta_{2k-1}(\theta) = \sum_{k=1}^{\infty} a_k^>, \quad (\text{B16})$$

the summation term has an asymptotic behavior of

$$a_k^> \stackrel{k \rightarrow \infty}{\sim} \frac{(-1)^k 4\sqrt{\pi}}{k} \frac{\Gamma(4k)}{\Gamma(2k)\Gamma(2k+1)} \left(\frac{e^{-\xi}d}{2M}\right)^{2k+1} \frac{r^2 [e^{-2ki\theta} + ie^{(2k-1)i\theta}]}{d(1+e^{-\xi})^2} \sqrt{\frac{1-e^{2i\theta}}{1-e^{-2\xi}}} \quad (\text{B17})$$

At $\theta = \pi/2$, we find

$$L = \lim_{k \rightarrow \infty} \left| \frac{a_{k+1}^>}{a_k^>} \right| = \left(\frac{2e^{-\xi}d}{M}\right)^2 = \left(\frac{2d}{M}\right)^2 \left[\frac{r - \sqrt{r(r-2M)}}{M} - 1 \right]^2, \quad (\text{B18})$$

which gives the same radius of convergence as in Eq. (57), such that $L < 1$ for every $r > d_o$. In both solutions, we did not show convergence at exactly $r = d_o$ for all θ , but this can be verified numerically.

2. Normalization constant

Now that we have already established the convergence of the solutions, we determine the normalization constant in the inner solution by enforcing continuity at the common radius of convergence. In principle, the normalization constant should be independent of θ . Hence, we fix the angle at $\theta = \pi/4$, and obtain a rapidly convergent summation terms that allows us to arrive at an approximate expression of C .

We rewrite the outer solution at $(r = d_o, \theta = \pi/4)$ as

$$\psi^>(r = d_o, \theta = \pi/4) = \sum_{m=1}^{\infty} b_m^{\text{odd}} + \sum_{n=1}^{\infty} b_n^{\text{even}}, \quad (\text{B19})$$

$$b_m^{\text{odd}} = -\frac{1}{2\sqrt{\pi}} \frac{\Gamma(2m - \frac{3}{2})}{\Gamma(2m)} d^{4m-2} R_{4m-3}^>(d_o) \left[\Theta_{4m-3}\left(\frac{\pi}{4}\right) - 1 + \frac{1}{\sqrt{2}} \right], \quad (\text{B20})$$

$$b_n^{\text{even}} = -\frac{1}{2\sqrt{\pi}} \frac{\Gamma(2n - \frac{1}{2})}{\Gamma(2n+1)} d^{4n} R_{4n-1}^>(d_o) \left[\Theta_{4n-1}\left(\frac{\pi}{4}\right) - 1 + \frac{1}{\sqrt{2}} \right]. \quad (\text{B21})$$

At $r = d_o$, we have the identity $e^{-\xi} = \frac{M}{2b}$. Then, the asymptotic behavior of the radial part is

$$R_{2k-1}^>(d_o) \stackrel{k \rightarrow \infty}{\sim} 32 \sqrt{\frac{2\pi}{k}} \frac{\Gamma(4k)}{\Gamma(2k+1)\Gamma(2k-1)} \left(\frac{1}{4d}\right)^{2k+1} \frac{d_o^2 d^3}{(2d+M)^2 \sqrt{4d^2 - M^2}}. \quad (\text{B22})$$

Meanwhile, at $\theta = \pi/4$, the angular harmonics have the asymptotic form

$$\Theta_{2k-1}\left(\theta = \frac{\pi}{4}\right) \stackrel{k \rightarrow \infty}{\sim} \frac{(-1)^k}{2\sqrt{k}} \frac{\Gamma(k+1)}{\Gamma(k+\frac{1}{2})} \left[\sqrt{\sqrt{2}+1} \cos\left(\frac{k\pi}{2}\right) - \sqrt{\sqrt{2}-1} \sin\left(\frac{k\pi}{2}\right) \right]. \quad (\text{B23})$$

Using the Stirling's approximation $\Gamma(z) \stackrel{z \rightarrow \infty}{\sim} \sqrt{2\pi} z^{z-1/2} e^{-z}$ in Eqs. (B22) and (B23), the odd and even summation terms exhibit

$$b_m^{\text{odd}} \stackrel{m \rightarrow \infty}{\sim} c_m^{\text{odd}} \equiv \left[\frac{(-1)^m \sqrt{2(\sqrt{2}-1)} - 1 + \sqrt{2}}{m^{3/2} \sqrt{\pi}} \right] \chi, \quad b_n^{\text{even}} \stackrel{n \rightarrow \infty}{\sim} c_n^{\text{even}} \equiv \left[\frac{2\sqrt{2}-2 - (-1)^n \sqrt{2(\sqrt{2}+1)}}{2n^{3/2} \sqrt{\pi}} \right] \chi, \quad (\text{B24})$$

where we define χ as

$$\chi \equiv \frac{d_o^2 d^2}{(2d+M)^2 \sqrt{4d^2 - M^2}}. \quad (\text{B25})$$

From these asymptotic behaviors, the slow convergence of the series can be attributed to the weak $k^{-3/2}$ decay together with the alternating nature of the terms. To obtain an approximate value for the outer solution, we sum the asymptotic contributions from $m, n = 2$ to infinity, while retaining the exact first term of each contribution. Since the infinite sum of k^{-n} is the Riemann Zeta function $\zeta(n)$, and the infinite sum of $(-1)^{k-1}/k^s$ is the Dirichlet zeta function $\eta(s) = (1-2^{1-s})\zeta(s)$, we obtain

$$\sum_{m=2}^{\infty} c_m^{\text{odd}} = \frac{\alpha^2}{\sqrt{\pi}} \left[\frac{\sqrt{2}}{\alpha} - 1 + (1-\alpha)\zeta\left(\frac{3}{2}\right) \right] \chi, \quad \sum_{n=2}^{\infty} c_n^{\text{even}} = \frac{\alpha^2}{2\sqrt{\pi}} \left[-2 - \frac{\sqrt{2}}{\alpha} + (2+\alpha)\zeta\left(\frac{3}{2}\right) \right] \chi, \quad (\text{B26})$$

where $\alpha \equiv \sqrt{\sqrt{2}-1}$, and their sum is

$$\sum_{m=2}^{\infty} c_m^{\text{odd}} + \sum_{n=2}^{\infty} c_n^{\text{even}} = \frac{\alpha}{2\sqrt{\pi}} \left[\sqrt{2} - 4\alpha - (\alpha-4)\zeta\left(\frac{3}{2}\right) \right] \chi. \quad (\text{B27})$$

Hence, the outer solution has an approximate expression of

$$\begin{aligned} \psi^> \approx & \frac{\alpha}{2\sqrt{\pi}} \left[\sqrt{2} - 4\alpha - (\alpha-4)\zeta\left(\frac{3}{2}\right) \right] \chi + \frac{d^2}{4096M^7} \left[768(\sqrt{2}-1)M^5(M+d_o) \right. \\ & + 70(2\sqrt{2}-7)(2M^3+12M^2d_o-75Md_o^2+45d_o^3)Md^2 \\ & \left. + 3d_o^2 \log\left(1-\frac{2M}{d_o}\right) \left[128(\sqrt{2}-1)M^4 + 35(2\sqrt{2}-7)(24M^2-40Md_o+15d_o^2)d^2 \right] \right]. \quad (\text{B28}) \end{aligned}$$

We may apply the same procedure to the inner solution. However, we do not present the details here, and instead quote the resulting approximate expression,

$$\psi^< \approx C\alpha \sqrt{\frac{2}{\pi}} \left[-\sqrt{2} + \alpha^2 \zeta\left(\frac{3}{2}\right) \right] \chi + \frac{d_o^2}{896\sqrt{2}d^4} \left[40M^3 - 120M^2d_o + 105Md_o^2 + 112(2d_o-3M)d^2 - 28d_o^3 \right]. \quad (\text{B29})$$

The expression for C is then obtained by equating Eqs. (B28) and (B29). In the limit $d_o \gg M$ or $M \rightarrow 0$, C should approach unity, and our truncated expression gives $C \approx 0.964$.

[1] T. M. Heckman and G. Kauffmann, The coevolution of galaxies and supermassive black holes: A local perspec-

tive, *Science* **333**, 182 (2011).

- [2] D. Alexander and R. Hickox, What drives the growth of black holes?, *New Astronomy Reviews* **56**, 93 (2012).
- [3] B. Webster, J. H. Croston, B. Mingo, R. D. Baldi, B. Barkus, G. Gürkan, M. J. Hardcastle, R. Morganti, H. J. A. Röttgering, J. Sabater, T. W. Shimwell, C. Tasse, and G. J. White, A population of galaxy-scale jets discovered using LOFAR, *Monthly Notices of the Royal Astronomical Society* **500**, 4921 (2020).
- [4] J. Aleksić, E. A. Alvarez, L. A. Antonelli, P. Antoranz, M. Asensio, M. Backes, J. A. Barrio, D. Bastieri, J. Becerra González, and Bednarek, W. et al., MAGIC observations of the giant radio galaxy M87 in a low-emission state between 2005 and 2007, *A&A* **544**, A96 (2012).
- [5] J. Feng and Q. Wu, Constraint on the black hole spin of m87 from the accretion-jet model, *Monthly Notices of the Royal Astronomical Society* **470**, 612 (2017).
- [6] The E.H.T. Collaboration, K. Akiyama, J. C. Algaba, A. Alberdi, W. Alef, R. Anantua, K. Asada, R. Azulyay, A.-K. Baczko, D. Ball, and Baloković, Mislav et al., First M87 Event Horizon Telescope results. VIII. Magnetic field structure near the event horizon, *The Astrophysical Journal Letters* **910**, L13 (2021).
- [7] M. A. Abramowicz and P. C. Fragile, Foundations of Black Hole Accretion Disk Theory, *Living Rev. Rel.* **16**, 1 (2013), arXiv:1104.5499 [astro-ph.HE].
- [8] M. Liska, A. Tchekhovskoy, and E. Quataert, Large-scale poloidal magnetic field dynamo leads to powerful jets in GRMHD simulations of black hole accretion with toroidal field, *Mon. Not. R. Astron. Soc.* **494**, 3656 (2020), <https://academic.oup.com/mnras/article-pdf/494/3/3656/33145099/staa955.pdf>.
- [9] A. Tchekhovskoy, R. Narayan, and J. C. McKinney, Efficient generation of jets from magnetically arrested accretion on a rapidly spinning black hole, *Mon. Not. R. Astron. Soc. Lett.* **418**, L79 (2011).
- [10] R. D. Blandford and R. L. Znajek, Electromagnetic extraction of energy from Kerr black holes., *Mon. Not. R. Astron. Soc.* **179**, 433 (1977).
- [11] S. S. Komissarov, Blandford-Znajek mechanism versus Penrose process, *J. Korean Phys. Soc.* **54**, 2503 (2009), arXiv:0804.1912 [astro-ph].
- [12] R. L. Znajek, Black hole electrodynamics and the Carter tetrad, *Mon. Not. R. Astron. Soc.* **179**, 457 (1977).
- [13] R. Adhikari, G. Menon, and M. V. Medvedev, Nonnull and force-free electromagnetic configurations in Kerr geometry, *Phys. Rev. D* **109**, 024015 (2024).
- [14] T. D. Brennan, S. E. Gralla, and T. Jacobson, Exact solutions to force-free electrodynamics in black hole backgrounds, *Classical and Quantum Gravity* **30**, 195012 (2013).
- [15] V. S. Beskin, *MHD Flows in Compact Astrophysical Objects: Accretion, Winds and Jets*, *Astronomy and Astrophysics Library* (Springer, 2010).
- [16] S. E. Gralla, A. Lupsasca, and M. J. Rodriguez, Electromagnetic jets from stars and black holes, *Phys. Rev. D* **93**, 044038 (2016).
- [17] K. Tanabe and S. Nagataki, Extended monopole solution of the Blandford-Znajek mechanism: Higher order terms for a Kerr parameter, *Phys. Rev. D* **78**, 024004 (2008).
- [18] G. Grignani, T. Harmark, and M. Orselli, Force-free electrodynamics near rotation axis of a Kerr black hole, *Classical and Quantum Gravity* **37**, 085012 (2020).
- [19] T. Uchida, Theory of force-free electromagnetic fields. I. General theory, *Phys. Rev. E* **56**, 2181 (1997).
- [20] S. E. Gralla and T. Jacobson, Spacetime approach to force-free magnetospheres, *Mon. Not. R. Astron. Soc.* **445**, 2500 (2014).
- [21] G. Menon, The non-null and force-free electromagnetic field, *Classical and Quantum Gravity* **38**, 145018 (2021).
- [22] G. Compère, S. E. Gralla, and A. Lupsasca, Force-free foliations, *Phys. Rev. D* **94**, 124012 (2016).
- [23] D. A. Uzdensky, Force-free magnetosphere of an accretion disk - Black hole system. 2. Kerr geometry, *Astrophys. J.* **620**, 889 (2005).
- [24] J. F. Mahlmann, P. Cerdá-Durán, and M. A. Aloy, Numerically solving the relativistic Grad-Shafranov equation in Kerr spacetimes: Numerical techniques, *Mon. Not. Roy. Astron. Soc.* **477**, 3927 (2018).
- [25] M. H. P. M. van Putten and A. Levinson, Theory and astrophysical consequences of a magnetized torus around a rapidly rotating black hole, *Astrophys. J.* **584**, 937 (2003).
- [26] J. Armas, Y. Cai, G. Compère, D. Garfinkle, and S. E. Gralla, Consistent Blandford-Znajek expansion, *J. Cosmol. Astropart. Phys.* **2020** (04), 009.
- [27] K. Parfrey, D. Giannios, and A. M. Beloborodov, Black hole jets without large-scale net magnetic flux, *Mon. Not. R. Astron. Soc. Lett.* **446**, L61 (2014).
- [28] A. Bransgrove, B. Ripperda, and A. Philippov, Magnetic hair and reconnection in black hole magnetospheres, *Phys. Rev. Lett.* **127**, 055101 (2021).
- [29] B. Ripperda, F. Bacchini, and A. A. Philippov, Magnetic reconnection and hot spot formation in black hole accretion disks, *Astrophys. J.* **900**, 100 (2020).
- [30] I. V. Igumenshchev, Magnetically arrested disks and the origin of poynting jets: A numerical study, *The Astrophysical Journal* **677**, 317 (2008).
- [31] M. Nakamura, K. Asada, K. Hada, H.-Y. Pu, S. Noble, C. Tseng, K. Toma, M. Kino, H. Nagai, K. Takahashi, J.-C. Algaba, M. Orienti, K. Akiyama, A. Doi, G. Giovannini, M. Giroletti, M. Honma, S. Koyama, R. Lico, K. Niinuma, and F. Tazaki, Parabolic jets from the spinning black hole in M87, *Astrophys. J.* **868**, 146 (2018).
- [32] M. Ruiz, C. Palenzuela, F. Galeazzi, and C. Bona, The role of the ergosphere in the blandford-znajek process, *Mon. Not. R. Astron. Soc.* **423**, 1300 (2012).
- [33] K. Toma, F. Takahara, and M. Nakamura, On the mechanism of black hole energy reduction in the blandford-znajek process, *Prog. Theor. Exp. Phys.* **2025**, 033E02 (2025).
- [34] H. Bateman and B. M. Project, *Higher Transcendental Functions. Vol. I* (McGraw-Hill Book Company, 1953).